Atomistic simulations of the formation and destruction of nanoindentation contacts in tungsten

J. H. A. Hagelaar,[1] E. Bitzek,[2,*] C. F. J. Flipse,[1] and P. Gumbsch[2,3]
[1]*Department of Applied Physics, Eindhoven University of Technology, P.O. Box 513, 5600 MB Eindhoven, The Netherlands*
[2]*Institut für Zuverlässigkeit von Bauteilen und Systemen (izbs), Universität Karlsruhe (TH), Kaiserstrasse 12, 76131 Karlsruhe, Germany*
[3]*Fraunhofer-Institut für Werkstoffmechanik IWM, Wöhlerstrasse 11, 79108 Freiburg, Germany*
(Received 7 August 2005; revised manuscript received 16 November 2005; published 23 January 2006)

This paper presents atomistic simulations of contact formation, indentation, subsequent pulling, and contact failure between a tungsten tip and a tungsten substrate. Different combinations of [111] and [110] crystal directions parallel to the direction of indentation are investigated. The simulations are performed using a Finnis-Sinclair potential for tungsten and a displacement controlled, quasistatic simulation scheme. The simulation setup and the tip geometry are inspired by low temperature scanning tunneling microscope indentation-retraction experiments. In the case of identical crystalline orientation of tip and substrate, deformation during indentation and the early stages of retraction is carried exclusively by prismatic dislocation loops. When the so formed nanocontact between the tip and substrate gets smaller, the deformation mechanism changes to atomic rearrangements within the neck. For configurations with different crystallographic orientation of the tip and substrate, the deformation is mainly carried by local atomic rearrangements within the interface region. Failure of the contact always occurs at the interface. In all cases debris is leftover on the substrate. The simulation results are discussed in the framework of nanoindentation and contact failure. The importance of the atomistic structure of interfaces in nanoscale contact problems is highlighted.

DOI: 10.1103/PhysRevB.73.045425 PACS number(s): 62.20.Fe, 62.20.Qp, 62.25.+g

I. INTRODUCTION

The formation, deformation, and fracture of atomic-scale contacts between two material bodies are fundamental mechanisms involved in friction and wear processes.[1–3] As nanosized asperities are highly faceted and atomically structured, continuum-mechanic contact models might not be applicable. Furthermore, nanosize metallic contacts show interesting electronic transport properties. When the contact is of atomic size, transport through the contact becomes ballistic and shows material-dependent "quantized" features.[4] Nanocontacts therefore have been subject of intensive experimental studies, e.g., by mechanically controllable break junctions[5,6] (MCBJ) or scanning tunneling microscopy (STM).[7–11] In addition, atomistic studies have been performed on the formation of nanocontacts by nanoindentation and subsequent retraction,[11–16] as well as on the yielding of nanowires, see, e.g., Refs. 10, 11, and 17–22. For an overview of the experimental and simulation work on the deformation mechanisms, friction, and electronic conductance of atomic-sized contacts the reader is referred to the reviews.[4,23,24]

Although the limited time scale accessible to molecular dynamics (MD) simulations leads to high pulling rates and neglect of some temperature dependent processes,[4,23] MD simulations have been able to reveal nicely the dominant deformation mechanisms of nanocontacts in fcc metals. For large constrictions deformation takes place by alternating elastic elongation and subsequent slip events on close-packed {111} planes via individual Shockley partial dislocations that nucleate at the surface of the contact.[16,17,21] For thinner constrictions, homogeneous shear of one plane of atoms over another plane was observed.[21] Depending on the crystalline orientation, different slip planes can be active,[20,21] leading for example to three-plane slip.[21] During the last stages of deformation of an initially large nanocontact the nature of deformation changes and becomes similar to that of small constrictions:[11,14,17,20,21] between elastic loading stages the constriction becomes unstable and atomic structural rearrangements lead to a local disordering of the constriction which reorders with the introduction of a new atomic layer.

From the numerous MD simulations it is now well established that the abrupt jumps in the conductance seen in experiments are the results of sudden structural atomic rearrangements.[4,11,17,20,21] However, many questions remain, especially on the influence of the local geometrical tip structure and the interface between tip and substrate on the strength of the formed contact.[15,25] Furthermore, many simulations of contact formations were performed on fcc metals,[10,11,13,14,17,20,21] while bcc metals have not yet been studied extensively.

In the present paper, we report on atomistic simulations of a tungsten tip indenting in and subsequently retracting from a tungsten substrate. We focus on the mechanisms by which the tip and the resulting nanocontact deforms and on the influence of the interface between tip and substrate on the failure of the tip-substrate contact.

The simulation setup is chosen such that it mimics the indentation-retraction cycle of a STM tip at low temperatures. Tungsten was chosen as representative for a bcc metal not only because of its elastic isotropy but also because it is the most important probe tip material and because its use as wear improving coating in microelectromechanical system (MEMS).[26]

The outline of the present paper is as follows. Section II gives details about the simulation method. In Sec. III the results of the simulations are presented. The findings are discussed in Sec. IV in the framework of nanoindentation and contact failure. Section V gives a short summary.

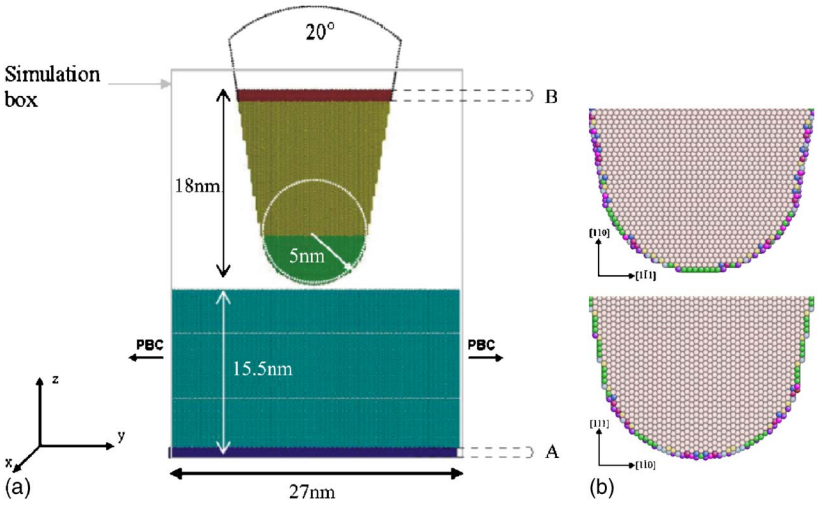

FIG. 1. (Color online) (a) The setup for the simulations, the details and dimensions are given in the text. (b) Details of the tip apexes. The [110] oriented tip (top) shows a flat terrace at the end, whereas the [111] oriented tip (bottom) exhibits no such terrace.

II. METHODS

In this work quasistatic atomistic simulations of the indentation-retraction cycle of a tungsten STM tip on a tungsten substrate are presented. Different combinations of the crystal directions [111] and [110] along the $\hat{z}$ direction of tip and sample are simulated.

Orientation I. A [111] oriented tip on a [111] oriented substrate, with the relative orientation $(111)_t \| (111)_s$; $[1\bar{1}0]_t \| [1\bar{1}0]_s$.

Orientation II. A [110] oriented tip on a [110] oriented substrate, with the relative orientation $(110)_t \| (110)_s$; $[1\bar{1}1]_t \| [1\bar{1}1]_s$.

Orientation III. A [111] oriented tip on a [110] oriented substrate, with the relative orientation $(111)_t \| (110)_s$; $[1\bar{1}0]_t \| [1\bar{1}1]_s$.

Orientation IV. A [110] oriented tip on a [111] oriented substrate, with the relative orientation $(110)_t \| (111)_s$; $[1\bar{1}1]_t \| [1\bar{1}0]_s$.

Orientation V. A [111] oriented tip rotated by 60° with respect to the [111] oriented substrate, resulting in the relative orientation $(111)_t \| (111)_s$;$[0\bar{1}1]_t \| [1\bar{1}0]_s$.

These directions are chosen because the [111] direction exposes a rather open structure and the [110] direction exposes the densest plane of atoms. In both configurations I and II the crystallographic orientation of tip and substrate is identical. Because of the lateral displacements the stacking sequence of the atoms, however, is not necessarily continuous between the tip and substrate, even if they have the same crystallographic orientation. The effect of lateral displacement is studied for orientation I. All the other orientations lead to interfaces that correspond to high angle grain boundaries. In configuration V the rotation around the common $\langle 111 \rangle$ direction results in a $\Sigma=3$ twist boundary upon contact.

The starting configuration that is used is similar for all simulations and is indicated in Fig. 1. The total number of atoms is about 835.000. The tip is a 18 nm high tungsten cone with an opening angle of 20° that is terminated with a semisphere with a 5 nm radius and consists of approximately 115.000 atoms. This radius of curvature is about the same as the sharpest tip that can be obtained experimentally.[27,28] The apex structure of the two different tips is shown in Fig. 1. The tungsten substrate consists of about 720.000 atoms and is 16 nm thick. Periodic boundary conditions are applied along the $\hat{x}$ and $\hat{y}$ directions. The total simulation box has the dimensions $27 \times 27 \times 35$ nm^3. The system size is comparable to that of recent nanoindentation simulations,[29–31] and significantly larger than previous indentation-retraction simulations.[12,14,16]

The tip and substrate are divided into three different regions, see Fig. 1. In regions A and B, the atom positions are prescribed and held constant to control the distance between the tip and substrate. The motion of the tip is achieved by shifting the atoms in region B in steps of 0.025 nm with respect to the substrate (region A). The atoms outside regions A and B are free to move at any time during the simulation.

The initial distance between the lowest atom of the tip and the uppermost atom of the sample is chosen to be 0.5 nm. Since the cutoff radius of the potential is 0.44 nm, there is initially no interaction between atoms of the tip and substrate. The displacement of the fixed tip atoms in region B (see Fig. 1) Δz_{tip} is used from there on to determine the tip-sample distance $z=0.5+\Delta z_{\text{tip}}$ nm. The total distance by which the tip is shifted towards the substrate is about 1 nm and thus the maximum indentation into the substrate is a little less then 0.5 nm. Experimentally, indentation depths of this order can be reached using scanning probe microscopes (SPMs).[7] The indentation is followed by a subsequent retraction until full detachment of the tip from the substrate.

All simulations are performed quasistatically. This means that after each shift of the tip towards the substrate, the system is relaxed to the (local) energy minimum. The so-called global convergence (gloc) algorithm is used here for minimization.[32,33] For the present problem it is generally converging somewhat faster than the conjugate gradient algorithm. The gloc algorithm works as follows: all N atoms in the system are moved freely according to the forces acting on them as in a classical molecular dynamics calculation until the $3N$ dimensional velocity vector $\vec{V}=(v_{1,x}, v_{1,y}, v_{1,z}, \ldots, v_{N,x}, v_{N,y}, v_{N,z})$ and the $3N$ dimensional force vector

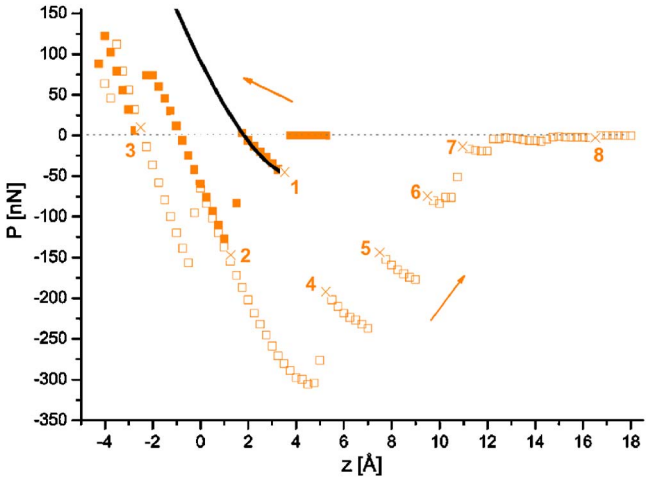

FIG. 2. (Color online) Load during indentation and subsequent retraction of the [111] oriented tip on the [111] oriented substrate (orientation I). The indentation part is indicated by filled squares and starts at a tip-sample distance of $z=0.5$ nm. Retraction starts at $z=-0.425$ nm and is indicated by open squares. The line starting at point 1 corresponds to the Hertz model with the reduced modulus of the potential and a tip radius of $R=5$ nm. The numbers referring to the crosses in the figure correspond to the numbering of the pictures in Fig. 3.

$\vec{F}=(f_{1,x},f_{1,y},f_{1,z},\ldots,f_{N,x},f_{N,y},f_{N,z})$ are antiparallel. At this point all velocities are set to zero.

If $\|\vec{F}\|\leqslant 10^{-6}$ eV/Å, the configuration is considered relaxed. After relaxation, the atoms are displaced and the configuration is relaxed again. This way, the quasistatic simulation mimics a displacement controlled, low temperature SPM indentation experiment.

The interatomic interactions are described by the semiempirical Finnis-Sinclair potential for tungsten.[34,35] The molecular dynamics simulations were performed using the ITAP molecular dynamics software package.[33] For visualization, the atomistic configuration viewer Atomeye[36] was used.

A graph of the calculated force as a function of the tip-sample distance is presented for the different orientations. It is accompanied by snapshots of the atomic configurations to illustrate the atomistic processes during deformation. The force P is calculated by adding up the $\hat{z}$ component of the force for all the atoms in region B. A negative force corresponds to an attraction between the tip and substrate.

III. RESULTS

A. Configurations with identical crystallographic orientation

1. Orientation I

The load as function of the tip-sample distance during indentation and subsequent tip retraction is plotted in Fig. 2. The arrows illustrate the direction of motion of the tip, and the numbers in Fig. 2 correspond to the numbers of the pictures in Fig. 3. The jump to contact at point 1 occurs at a tip-sample distance of $z_{\text{contact}}=0.35$ nm and leads to an attractive force of $P=-45$ nN. The following jump in the force at point 2 is caused by the nucleation of a prismatic dislocation loop at the contact between tip and substrate, and its subsequent motion within the tip along the $[11\bar{1}]$ direction to the surface of the tip (see picture 2 in Fig. 3). This process changes the tip-substrate interface from a head-on-head configuration to a perfect match. At point 3 a prismatic dislocation loop on the [111] glide cylinder nucleates (see picture 3 in Fig. 3). The nature and the process of formation of this interstitial prismatic dislocation loop is illustrated in Fig. 4: during the indentation the atoms at the end of the tip form an extra plane between tip and substrate. The radius of the prismatic dislocation loop is about 1.6 nm. The indentation is continued without further structural changes.

Upon retraction the load is not exactly following the load-displacement curve during the indentation. This is most probably due to the interaction of the prismatic dislocation loop with the substrate boundary. Between $z=-0.05$ and $z=0$ nm this dislocation disappears in the same way as it nucleated, leading to a jump in the force. The maximum attractive force of $P=-310$ nN is reached at a tip sample distance of $z=0.475$ nm. The following large jump in force (point 4) is due to the nucleation of a vacancy like prismatic dislocation loop at the tip-substrate contact (see picture 4 in Fig. 3), which moves down into the substrate along its [111] glide cylinder. The Burgers vector of this dislocation loop is opposite to that of the dislocation formed at point 3 (see Fig. 4), the radius ($r\approx 1.6$ nm) is the same. This process is repeated at the next jump in force (picture 5 in Fig. 3), leading to the generation of a second prismatic dislocation loop with smaller radius ($r\approx 1.3$ nm).

At point 6 the neck has deformed by slip along the $[11\bar{1}]$ direction on the (110) plane (picture 6 in Fig. 3). The force jump leading to point 7 is due to the disappearance of the dislocation loop formed at point 5 at the surface (along the [111] direction). This results in further narrowing of the neck.

The subsequent jumps in force are caused by local structural rearrangements in the neck, as depicted in Fig. 5. As the tip moves away from the substrate, extra layers parallel to the (110) plane form in the neck. These layers that are only a few atoms wide, are formed by atoms from neighboring planes. In Fig. 5 this is illustrated by dashed circles and arrows indicating the movement of the atoms before and after the formation of the extra layer. At a tip sample distance of $z=1.675$ nm the single atom contact breaks.

To show the transfer of material between tip and substrate, the configuration of picture 8 in Fig. 3 is shown in Fig. 6(a) with the color of the atoms corresponding to their origin. Consistent with the deformation by nucleation of prismatic loops corresponding to vacancy platelets in the substrate, the neck is formed almost completely out of atoms originally coming from the substrate.

2. Orientation II

The force-distance curve of the indentation-retraction cycle for the [110] oriented tip on the [110] oriented substrate is shown in Fig. 7. Figure 8 shows the configurations corresponding to the numbers indicated in Fig. 7.

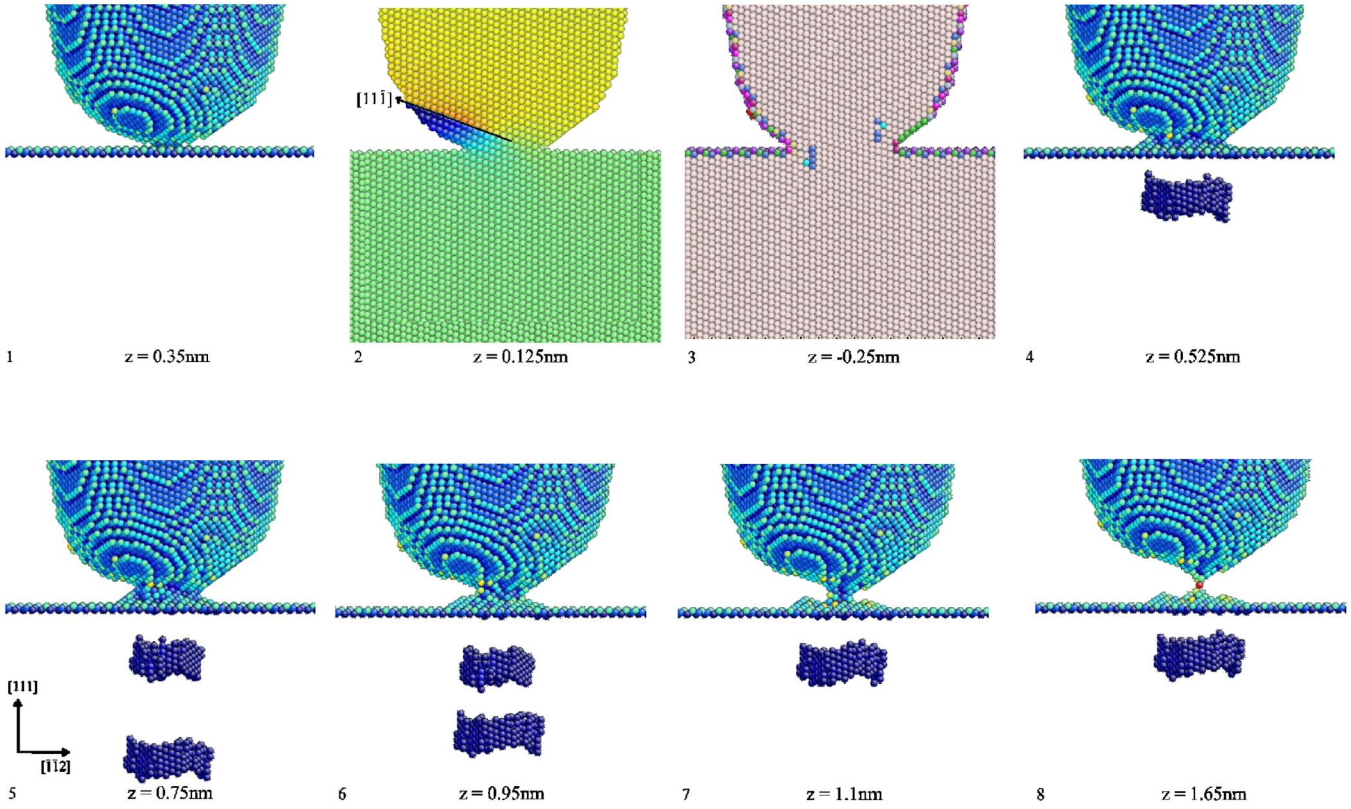

FIG. 3. (Color online) Snapshots of configuration I during the indentation-retraction simulation showing the nucleation of prismatic dislocation loops and formation of a single atom contact. The numbers of the pictures correspond to loads and displacements indicated in Fig. 2. The atoms in all the pictures are color coded according to potential energy except for pictures 2 and 3, which show a cut through the configuration. In picture 2 the color corresponds to the atomic displacement in $[\bar{1}\bar{1}2]$ direction (blue: displacement by 2.2 Å to the right, red: displacement by 2.2 Å to the left), thus tracing the passage of the prismatic dislocation loop. The atoms in picture 3 are color coded according to their coordination number. The blue atoms in the contact show the interstitial prismatic dislocation loop that nucleated.

The jump to contact takes place at $z_{\text{contact}}=0.425$ nm, and leads to an attractive force of $P=-94$ nN (see Fig. 7). The next jump in force, point 1 in Figs. 7 and 8, is caused by the nucleation of an interstitial prismatic dislocation loop with $[11\bar{1}]$ glide cylinder at the contact between the tip and sample. Upon further indentation the upper and lower parts of the dislocation loop glide in opposite directions, leading to a change in the angle between the plane of the loop and the substrate from ~0° to ~90°. At the jump in force between $z=-0.1$ and $z=-0.125$ nm, the Burgers vector of the loop flips and the glide cylinder changes accordingly from $[11\bar{1}]$ to $[\bar{1}\bar{1}\bar{1}]$. This allows the loop to leave the tip along the $[\bar{1}\bar{1}\bar{1}]$ direction near the contact leading to an additional increase in contact area. In Fig. 9(a) this process is visualized by color coding the atomic displacements between the configurations at $z=-0.1$ and $z=-0.125$ nm. The flip is probably caused by the strong gradient in the stress field within the contact region. Such Burgers vector flips of interstitial loops are commonly observed in studies of irradiation-induced hardening,[37] where the flipping usually is thermally activated. The two subsequent jumps in the force are caused by the nucleation of prismatic dislocation loops with $[111]$ and $[11\bar{1}]$ glide cylinders. Both dislocations glide within the tip, however, the indentation is stopped before the last loop reaches the tip surface.

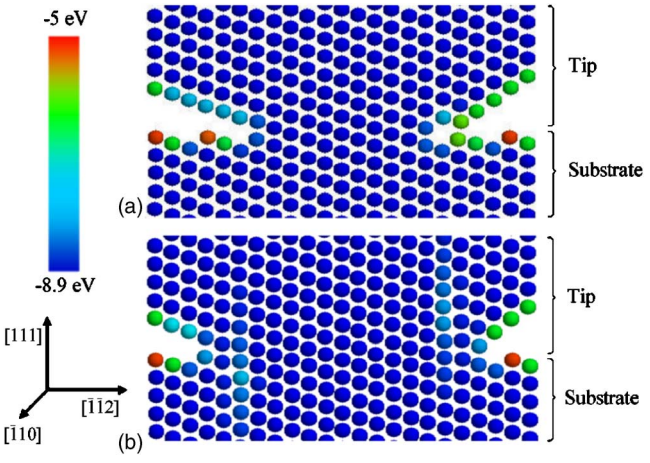

FIG. 4. (Color online) Nucleation of the prismatic dislocation loop during indentation of configuration I. In (a), the continuous crystallographic relationship between tip and substrate can be seen. At point 3 in Fig. 2 one atomic plane is pushed in between tip and substrate forming a prismatic dislocation loop. This is illustrated in (b). The color represents the potential energy of the atoms.

Upon retraction the dislocation loop first moves back to the tip-sample contact, where it annihilates. This leads to a

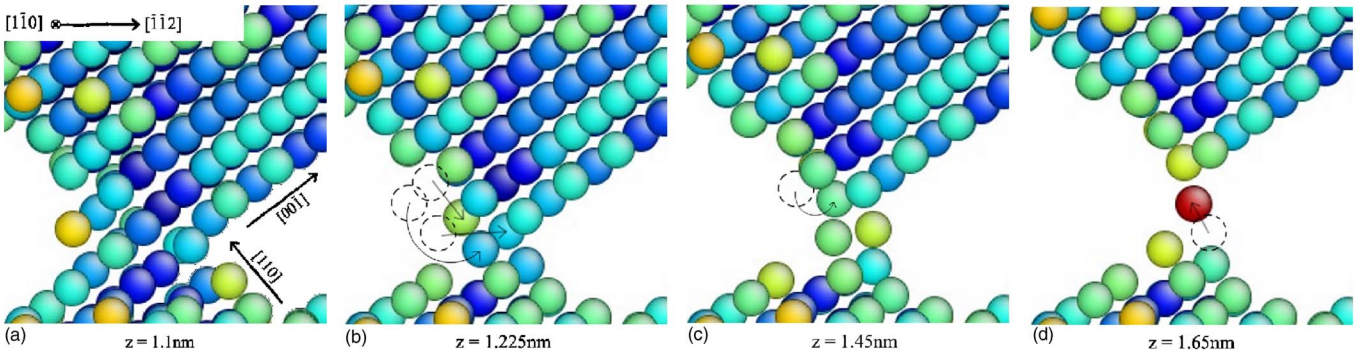

FIG. 5. (Color online) Different stages of breaking of the atomic contact in orientation I; color indicates the coordination number. Each of the pictures is a snapshot taken just after a plastic event. (a) Zoom on the neck of picture 7 in Fig. 3. In the pictures the displacement of the atoms is illustrated by dashed circles and arrows.

change in the slope ($z=-0.15$ nm) of the load-displacement curve, Fig. 7.

The retraction curve (Fig. 7) shows many jumps in the force. Most of these jumps are caused by the nucleation of vacancy-type prismatic dislocation loops with glide cylinder orientation alternating between $[111]$ and $[11\bar{1}]$. These orientations allow the dislocation loops to leave the tip. Nucleation, glide, and annihilation of the dislocation at the surface can take place during one displacement step. The motion of the dislocation has therefore to be traced by the atomic displacements between the configurations before and after the jump in force, see Fig. 9(b). Each time a prismatic dislocation loop reaches the surface of the tip, a step is formed at the tip surface.

At point 2 in Fig. 8 a prismatic dislocation loop moves into the substrate along the $[\bar{1}\bar{1}1]$ direction instead of moving in the tip. It moves to the tip surface after the tip is deformed by a prismatic loop gliding in the $[11\bar{1}]$ direction.

At point 3 two loops simultaneously move down into the substrate along the $[\bar{1}\bar{1}\bar{1}]$ and the $[\bar{1}\bar{1}1]$ directions, forming a $\boldsymbol{b}=a/2[00\bar{2}]$ sessile dislocation at the intersection of their glide cylinders. The configuration at point 4 shows a similar loop within the tip (see Fig. 9(c)), from the reaction $\boldsymbol{b}=a/2[\bar{1}\bar{1}1]+a/2[111]=a/2[002]$.

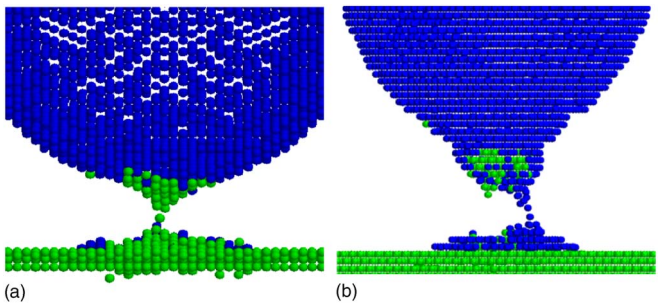

FIG. 6. (Color online) The final configurations after tip retraction. (a) orientation I, corresponding to picture 8 in Fig. 3, (b) orientation II, corresponding to picture 8 in Fig. 8. The atoms are color coded according to their origin: blue (dark) atoms are originally coming from the tip whereas green (light) atoms come from the substrate.

Various dislocation processes including the nucleation of prismatic half loops in $[1\bar{1}1]$ and $[1\bar{1}\bar{1}]$ directions (parallel to the xy plane) occur during further retraction to point 5. Reactions of these loops with the $\boldsymbol{b}=a/2[00\bar{2}]$ dislocation lead to the formation of a small pore just underneath the neck (see picture 5 in Fig. 8, and 9(d)). Further reactions of prismatic dislocation loops on $[111]$ and $[11\bar{1}]$ glide cylinders (at $z=2.45$ nm and $z=2.85$ nm) lead to growth of the pore, which eventually leaves three separated necks (see picture 6 in Fig. 8). The necks then deform similarly to the neck in orientation I by insertion of extra (110) layers in the contact. This is indicated in pictures 7 and 8 of Fig. 8. Figure 6(b) shows the origin of the atoms in the final configuration. Consistent with the deformation by nucleation of vacancy-type prismatic loops, the neck is almost completely formed out of atoms from the tip.

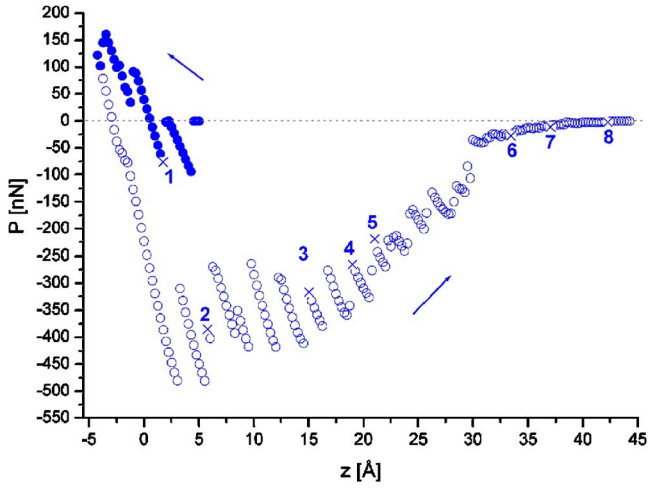

FIG. 7. (Color online) Load as function of displacement during the indentation (filled circles) and retraction of the [110] oriented tip from the [110] oriented substrate (orientation II). Indentation starts at a tip-sample distance of $z=0.5$ nm. Retraction (open circles) starts at -0.425 nm. The numbers referring to the crosses in the figure correspond to the numbers of the pictures in Fig. 8.

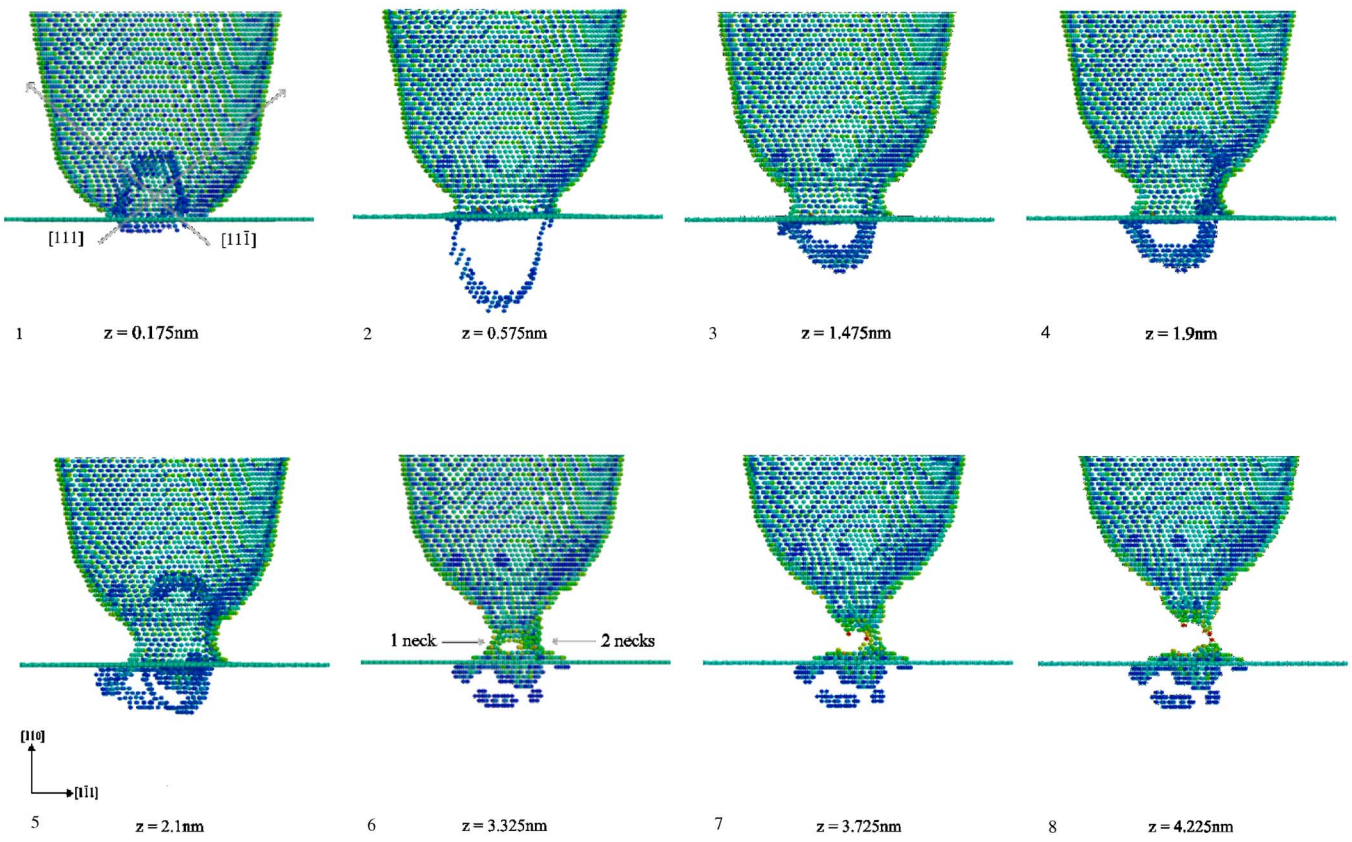

FIG. 8. (Color online) Snapshots of configuration II during the indentation-retraction simulation showing the formation of a single atom nanocontact. Only atoms with high potential energy are shown. The numbers of the pictures correspond to the numbers indicated in Fig. 7.

B. Configurations with different crystallographic orientations

1. Indentation

The indentation part of the load-displacement curves of all three misoriented configurations are shown in Fig. 10. As expected from the isotropy of the elastic constants, the overall magnitude of the load response is similar for all cases studied. However, the load-displacement curves for the nonmatching cases show more complexity as compared to the curves of the configurations with identical crystallographic orientation (Figs. 2 and 7). Also, the jump to contact instability can be much less pronounced in the nonmatching cases. For example, the [111] oriented tip does not show flat terraces at the apex (see Fig. 1). Thus when it indents the flat (110) substrate (configuration III), only some individual tip atoms make contact with the surface (z_{contact}=0.4 nm). For orientation IV the interface between tip and substrate is nominally the same as in orientation III. However, the existence of the terrace at the tip apex leads to a pronounced jump to contact, which is associated with atomic displacements u (up to $u \approx 0.27$ nm) within the terrace and a small elastic deformation of the tip. In this orientation the second terrace induces a second jump to contact (at z=0.2 nm).

The main deformation mechanisms for all nonmatching configurations are atomic displacements within the interface region. It is important to point out that, although certain regions of the load-displacement curves in Fig. 10 are nicely continuous and therefore seem to be purely elastic, irreversible local atomic rearrangements (displacements of the order of 1 Å) can take place within the interface. Larger atomic displacements in the interface region can cause significant load drops in all nonmatching configurations. If the atomic rearrangements are correlated, they are accompanied by elastic tilting or rotation of the tip. The emission of a dislocation half-loop was only observed in orientation IV.

The interface between indenter and substrate is not comparable to a clean grain boundary, even in the load-free state (first row in Fig. 12). The defective structure can extend up to roughly three atomic layers into the tip and substrate. Nearly all atomic displacements take place in this active zone. However, the defective zone extends into the tip rather than into the substrate. In orientation V this even leads to a motion of the interface plane towards the tip by one atomic layer. Displacements localized within the defective region at the interface can lead to a local bulging of the interface (see Fig. 12, orientation III).

2. Retraction

The load as function of the tip retraction is shown in Fig. 11. The atomic configurations of the interfaces during retraction are shown in Fig. 12.

At the beginning of the retraction, all configurations show a steady decrease of the applied load with approximately the same slope. During this stage the deformation is mainly carried by small atomic displacements within the interface region.

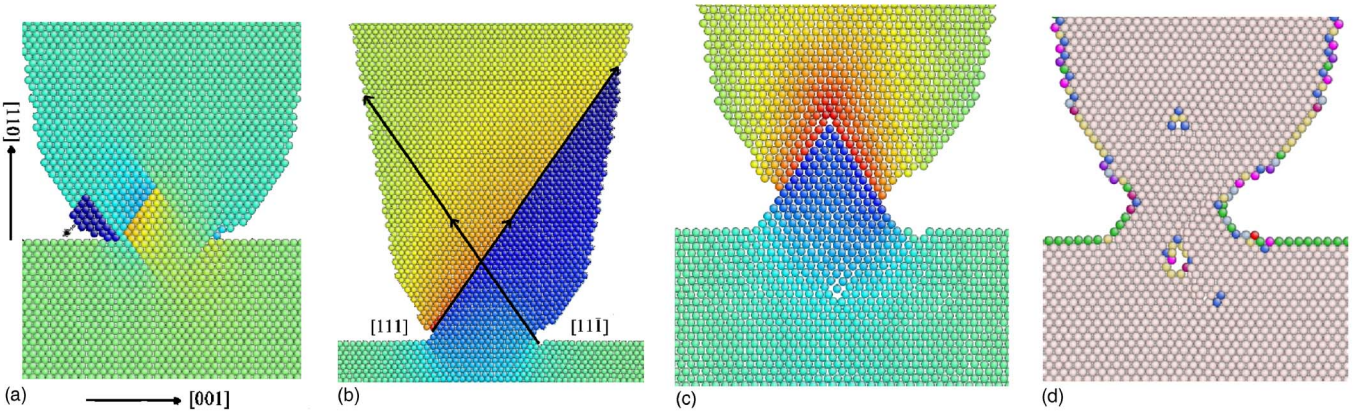

FIG. 9. (Color online) Vertical one atom thick slices of orientation II. (a) The Burgers vector flip at $z=-0.125$ nm of the prismatic dislocation loop can be traced by the atomic displacements in the [110] direction (blue indicates a downward displacement by max. −3.1 Å, red corresponds to an upward displacement by max. +3.1 Å) The arrow indicates the accompanied motion of the (blue) atoms. (b) The displacements in the [110] direction [blue atoms moved down (max. 1.8 Å), red atoms up (max. 1.8 Å)] tracing the glide of a vacancy type prismatic dislocation loop in the [111] direction through the tip ($z=0.325$ nm). Both active glide directions are indicated by black lines in the figure. (c) The displacements in [110] direction [blue atoms moved down (max. 1.5 Å), red atoms up (max. 1.5 Å)] just after the reaction of two prismatic dislocation loops in the tip (point 4 in Fig. 8). (d) Close-up on the void formed in the substrate at point 5 in Fig. 8. Color coding represents the coordination number of the atom.

Upon further retraction the force reaches a minimum. The maximal adhesive force sustained by the interface varies between $P\approx-256$ nN (orientation V) and $P\approx-219$ nN (orientation IV), see Table II. This maximal attractive force of course depends on the indentation depth from which the retraction started. Indenting orientation V only up to $z=-0.1$ nm ($P\approx0$ nN) gives a maximal attractive force during retraction of only $P\approx-160$ nN. The results of this simulation will be referred to as configuration V′.

The large jumps in the force upon retraction beyond the minimum all correspond to the failure of the contact. How the interface fails depends on the nature of the interface. Orientations V and IV show one smaller force jump ($\Delta P\approx30$ nN) followed by a large jump $\Delta P\approx110-140$ nN. The first jump is caused by the correlated displacement of 5–10 atoms over distances of up to 0.4 nm. These atoms are clustered at the circumference of the interface, the interface area is reduced by the rearrangements of the atoms. The second, larger jump is caused by the detachment of a part of the interface, resulting in the formation of thin necks between the tip and substrate. These necks fail one after the other.

Orientation III fails in a more continuous way and shows three subsequent jumps of $\Delta P\approx30-40$ nN. The first jump involves atoms within the interface region and results in the emergence of small voids. The voids then grow at the second jump. The third jump is caused by rearrangements of atoms at the circumference of the larger of the two remaining contacts. The tip in configuration V′ was only indented to $z=-0.1$ nm and therefore was only very little deformed. Consequently, the processes during retraction differ significantly

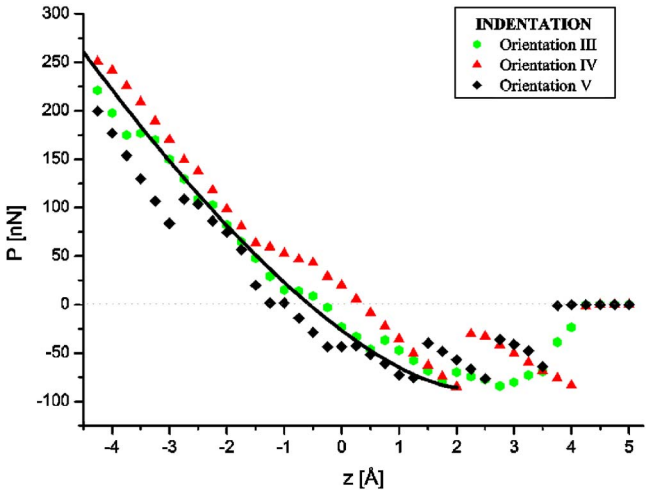

FIG. 10. (Color online) Load-displacement curve during the indentation with nonmatching tip-substrate configurations. The line corresponds to the Hertz model with tip radius $R=5$ nm. An offset is used to account for the attractive forces.

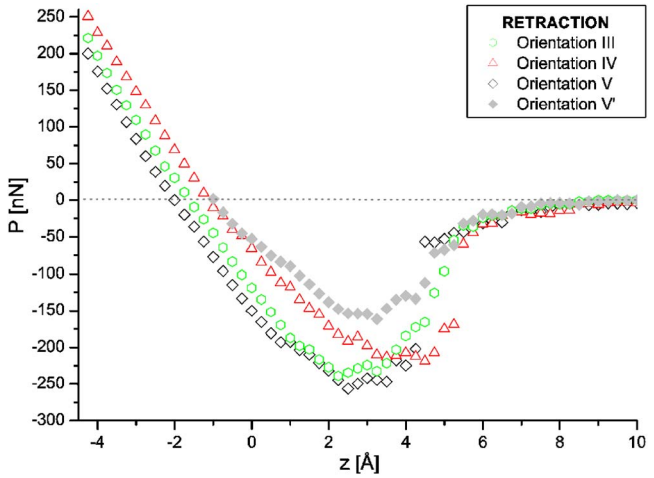

FIG. 11. (Color online) The retraction part of the load-displacement curves for the configurations with different crystallographic orientations.

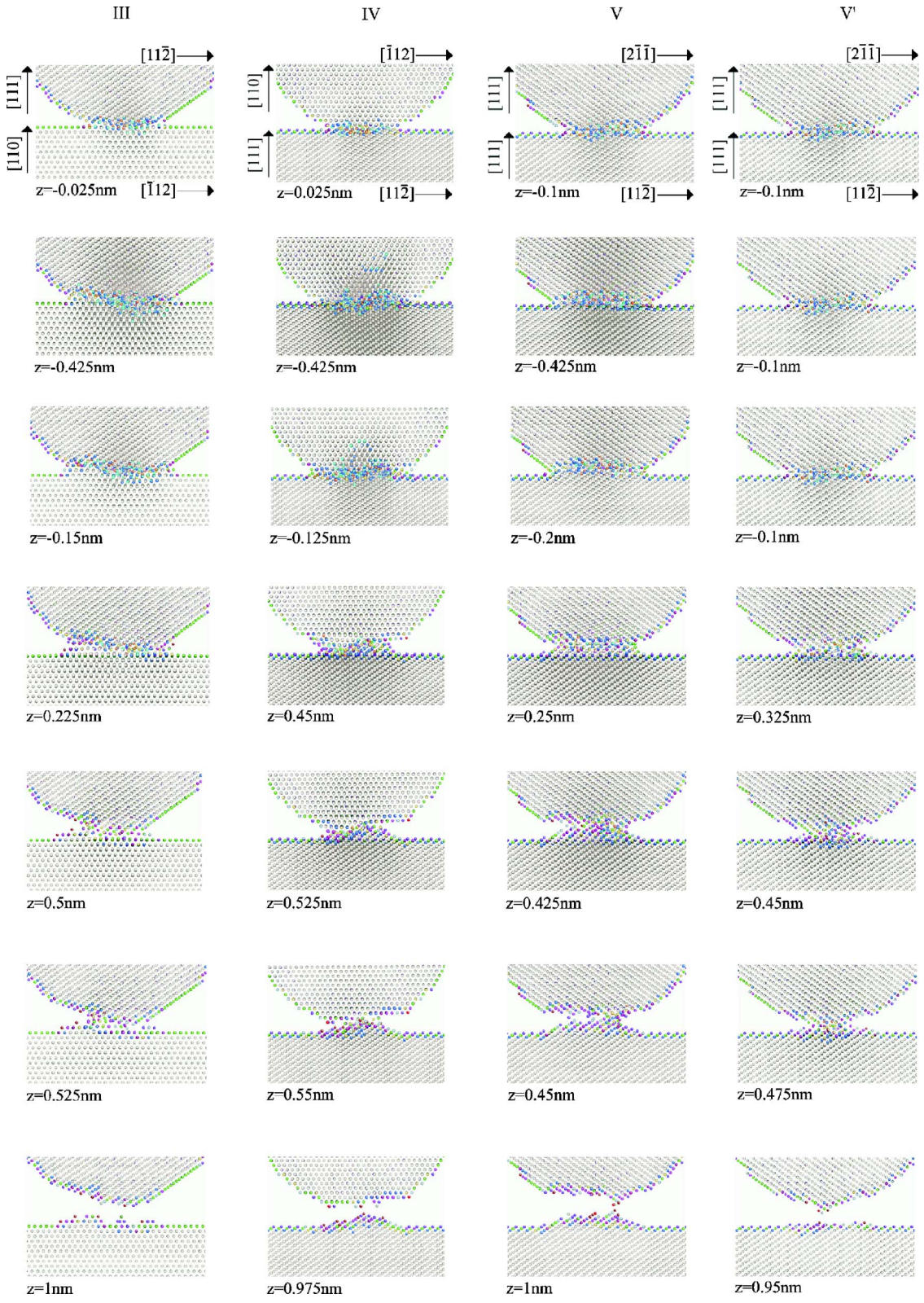

FIG. 12. (Color online) Evolution of the indenter-substrate interface during indentation and subsequent tip retraction for the setups with differing crystallographic orientations. The atoms are colored according to their coordination number. From top to bottom the following configurations are displayed: at zero load during indentation ($P_{\mathrm{ind}} \approx 0$), at maximum indentation depth, at zero load during retraction ($P_{\mathrm{retr}} \approx 0$), at maximum tensile load P_c, before and after the jump in the force (Fig. 11), and the final configuration. The according z values are different for the different configurations and are shown for each individual snapshot.

from those at deeper indentation (configuration V). Here, the interface shrinks from the circumference. Atomic rearrangements at the interface lead to a gradual reordering of the interface structure.

It is interesting to point out that material was transferred from the tip to the substrate in all the configurations that were significantly indented. The material transferred amounts to 300 tip atoms in orientation V (with three atoms transferred from the substrate to the tip), 302 atoms for orientation IV (two atoms transferred in opposite direction), and 103 atoms (orientation III) where there were, however, 49 atoms transferred from the substrate to the tip. The shallow indentation in the orientation V′ shows a nearly symmetric exchange of atoms: 29 tip atoms transferred to the substrate versus 23 substrate atoms transferred to the tip.

IV. DISCUSSION

A. System size and potential considerations

The imposed boundary conditions and details of the atomic interaction potential can in general have considerable influence on the results of atomistic simulations.

Compared with other atomistic indentation simulations[29–31,38] our sample size is rather large. Nevertheless, the fixed atoms along $\pm\hat{z}$, as well as the periodic boundary conditions in $\hat{x}$, $\hat{y}$ will lead to an elastically stiffer system compared to a real system. However, only very shallow indentations were performed here. The indentation depth was less than 10% of the sample height, and the maximum contact radius less than 10% of the sample size. Under such conditions the effect of the boundary conditions on the elastic properties of the sample can be neglected.[38]

The influence of boundary conditions in nanoindentation simulations on the plastic behavior of the substrate is more severe. It was discussed by Choi *et al.*[38] in some detail. Fixed boundary conditions, which model an infinitely stiff substrate, lead to repulsion of dislocations. Dislocations nucleated during the indentation in the substrate thus stay closer to the tip, the overall load-displacement relation is less compliant, and the simulated substrate film hardens more readily compared to larger systems.

For the retraction part of our simulation similar arguments apply. For orientation I, where dislocations were observed only in the substrate, the nucleation of more prismatic dislocation loops and therefore a more pronounced neck formation might be possible in a larger substrate. In the case of the [110] oriented tips the effect of the fixed boundary plays a minor role, since most of the dislocations escape through the tip surface or react with each other close to the contact region. One can therefore conclude that the applied boundary conditions might affect the total length of the formed contacts, but will not change the underlying deformation mechanisms, which are the main focus of the present study.

Whether an atomic scale contact forms or not also depends on the details of the atomic interaction potential. In order to compare our results which were obtained using the semiempirical Finnis-Sinclair (FS) potential[34,35] with a more accurate description of the atomic bonding, some simulations were performed using a bond order potential (BOP).[39,40] Relaxation of the central part of the nanocontact during the final stages of the retraction of the [111] oriented tip from the [111] substrate with BOP showed no significant structural differences compared to the FS calculations. The only significant difference is that the monatomic contact (picture 8 in Fig. 3), breaks in the BOP calculation at $z=1.625$ nm, while the contact snaps between $z=1.65-1.675$ nm in the FS calculation.

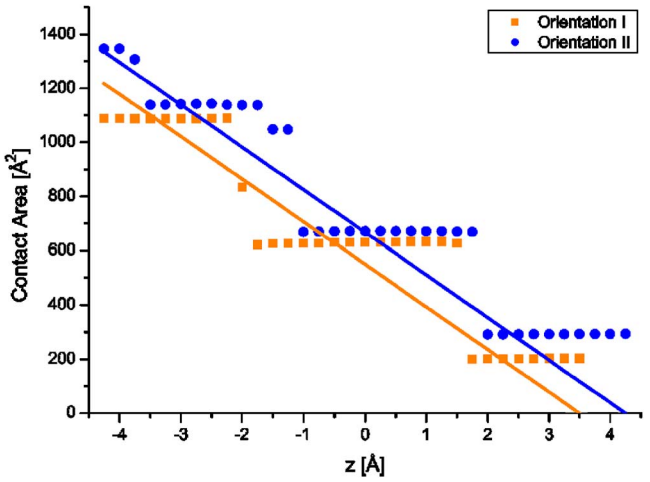

FIG. 13. (Color online) Evolution of the contact area A during indentation, for tips having the same crystallographic orientation as the substrate. For comparison with the Hertz solution (solid lines) A_c is plotted over the indentation depth $z_{\text{indent}}=z-z_{\text{contact}}$ starting at the jump to contact.

The use of the Finnis-Sinclair potential therefore seems to provide a realistic description of the processes during the formation of nanocontacts. A quantitatively correct description of the fracture of nanocontacts was not intended in this study.

B. Discussion of the indentation process

Common features of the indentation process in all the studied tip-substrate configurations are the jump to contact and the elastic deformation of the tip and substrate until plastic deformation relieves the accommodated stress. Further indentation takes place by subsequent phases of elastic loading and plastic deformation. Although the studied configurations share the same elastic (due to the isotropy of W) and geometrical properties, the characteristics of the indentation process differ significantly.

As additional information to the force-displacement plots (Figs. 2, 7, and 10), the contact area is plotted versus the tip-sample distance in Figs. 13 and 14. The contact area is calculated using the effective contact radius a, which is determined by the following expression:

$$\frac{a^2}{2}=\frac{\Sigma_i[(x_i-x_c)^2+(y_i-y_c)^2]}{N}, \tag{1}$$

designed to yield the correct radius for a circular geometry.[41] Here, the sum is over all N atoms in the uppermost layer of the substrate which have a lower energy than the surface

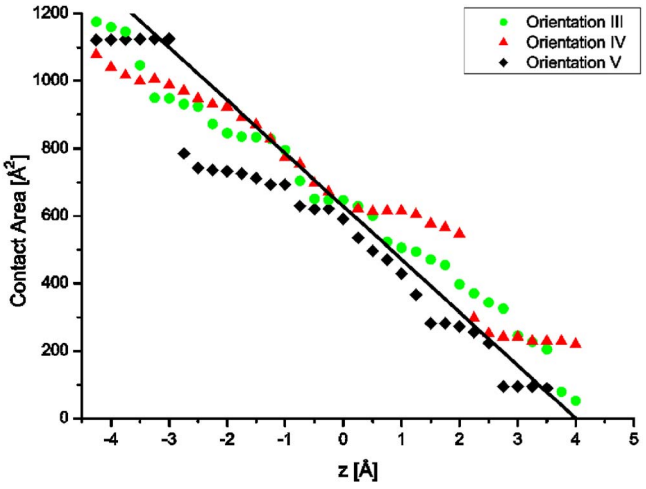

FIG. 14. (Color online) Same as Fig. 13, only for configurations with tip and substrate having different crystallographic orientations.

atoms. The center of mass of all of these atoms has the coordinates x_c and y_c.

Depending on the crystallographic orientation of tip and substrate, the jump to contact takes place at tip-sample distances ranging from $z_{\text{contact}}=0.35$ nm to $z_{\text{contact}}=0.425$ nm. These values agree well with the distances $z\approx 0.3-0.5$ nm, at which the jump to contact takes place in MCBJ experiments on tungsten.[6] The magnitude of the force jump associated with the jump to contact (see Figs. 2, 7, and 10) is mainly influenced by the size of the newly formed contact area (see Figs. 13 and 14). The size of the contact area depends directly on the atomic structure of the tip apex (see Fig. 1). Consequently, the jump in force is dominated by geometry rather than surface or interface energy.

The overall elastic response of the systems following the jump to contact instability compares well with the Hertz theory, which relates the applied load P to the indenter displacement $h=z-z_{\text{contact}}$:

$$P=\frac{4}{3}E^{*}R^{1/2}h^{3/2} \tag{2}$$

(R is the radius of curvature of the tip). However, the attractive force $P_c(z=z_{\text{contact}})$ at the jump to contact has to be used as an offset (see Figs. 2 and 10). The reduced modulus E^{*} is defined as

$$E^{*}=\left(\frac{1-\nu_s^2}{E_s}+\frac{1-\nu_i^2}{E_i}\right)^{-1}, \tag{3}$$

where $E_{i,s}$ is the Young's modulus and $\nu_{i,s}$ the Poisson ratio of the indenter, respectively, substrate. Due to the isotropy of tungsten [anisotropy constant $A=2c_{44}/(c_{11}-c_{12})=0.998$], the same reduced modulus $E^{*}=222$ GPa can be used for the discussion of the different indenter-substrate configurations. The solid line in Figs. 13 and 14 is the Hertzian contact area $A_c=\pi Rh$ associated with the elastic contact. The size of the contact area determined from the atomistic simulations compares well with the continuum mechanical expression. For identical crystallographic orientation of tip and substrate, the Hertzian expression for the load holds only up to the first plastic event. For configurations with different crystallographic orientations the deformation is dominated by small atomistic rearrangements in the interface region which results in a nearly continuous increase of contact area (Fig. 14) during indentation. For these configurations the load during indentation follows reasonably well the Hertzian expression (see Fig. 10).

The question of how atomistic details of interfaces influence contact problems, friction, wear, and plasticity at the nanoscale has recently attracted interest.[15,25,42] As an example, for the consequences of different atomic interface structures, we discuss here the nucleation of dislocations at the tip-substrate interface in nanoindentation simulations.

Many nanoindentation simulations use simplified assumptions to model the indenter-substrate interface. Simulations using a rigid atomistic tip neglect the details of the interface structure caused by elastic tip tilting or twisting. Furthermore, most simulations model the indenter using a spherical potential (e.g., Refs. 29–31 and 38), thus not taking into account the atomistic structure of the indenter and of its interface to the substrate. These simulations generally show the nucleation of dislocation loops within the substrate at a depth consistent with the location of the maximum resolved shear stresses predicted by the Hertzian theory. However, simulations with a spherical indenter indenting on a one atomic layer high surface step[31] showed nucleation of dislocations at the step. This is a strong indication that any irregularity, and in particular atomic steps at the interface between tip and substrate, significantly affect the nucleation of dislocations during nanoindentation.

The influence of the interface on the nucleation of dislocations in our simulations is best exemplified by the different processes taking place during the indentation with [111] oriented tips. Due to the isotropy of tungsten, all the simulated systems are elastically equivalent. As the same tip is used, and the dislocation in picture 2 of Fig. 3 only moves within the tip, the simulations with configurations I, III, and V have the same glide systems. However, only for the configuration I, with identical crystallographic orientation of tip and substrate we have the emission of two dislocations in the tip, the other configurations show at the same indentation depth only atomic rearrangements at the interface between tip and substrate. The first dislocation in configuration I removes the high energy stacking fault between tip and substrate. For such configurations with no perfect match between identically oriented tip and substrate there is an additional driving force to relieve the stress together with the mismatch by the nucleation of dislocations. A matching crystallographic orientation (orientations I and II) helps to create a layer of interstitial atoms at the contact, which then transforms into a prismatic dislocation loop (see Fig. 4). However, the observed dislocation nucleation in orientation IV demonstrates that an identical crystallographic orientation of tip and substrate is not necessary for the nucleation of dislocation loops. Figure 15 shows that atomic steps act as stress concentrators and thereby facilitate the nucleation of the dislocation at the interface. However, a critical stress concentration or a critical resolved shear stress required for the nucleation of a prismatic loop cannot easily be determined from the atomistic stresses in Fig. 15.

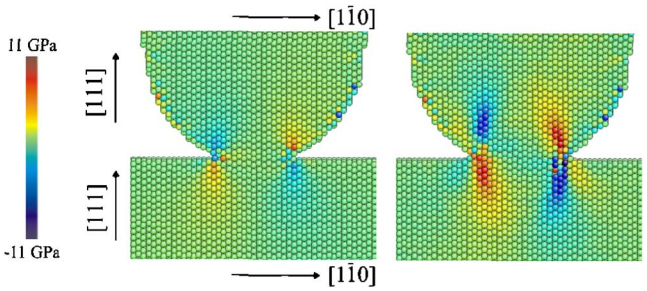

FIG. 15. (Color online) The local shear stresses σ_{xz} just before and just after the nucleation of the second prismatic dislocation loop in orientation I at point 3 in Fig. 3. The nucleation of this dislocation loop relieves the accumulated stress σ_{zz}, causing the load drop at point 3 in Fig. 2.

Within the context of dislocation nucleation at the indenter-substrate interface it is interesting to refer to the nanoindentation experiments of Kramer *et al.*[43] on single crystalline W. These experiments showed limited, occasionally reversible, plastic deformation at loads as low as one quarter of the critical yield point load. It was hypothesized that this phenomenon could be due to the nucleation of dislocations from the surface or interface to the indenter.[43,44]

C. Discussion of the processes during tip retraction

The deformation mechanisms are basically the same as during indentation. These are nucleation and slip of prismatic dislocation loops in the cases where tip and substrate share the same crystallographic orientation, versus atomic rearrangements in the nonmatching cases. Due to their different tendency to neck formation, both cases are discussed separately.

1. Configurations with identical crystallographic orientation

In both cases, retraction starts when there is still a prismatic dislocation loop left from indentation process. The first part of the retraction process is basically a reversal of the last indentation steps. The force plots (Figs. 2 and 7) have almost the same slope as during the last part of the indentation. In general, the process during indentation is reversible as long as the dislocations are still stored in the configuration and have not reacted with each other. Prismatic dislocation loops are bound to their glide cylinder and therefore have a lower probability to react with other dislocations than expanding glide loops. The reversibility of the indentation process thus depends on the deformation mechanism, the available glide systems, and the size and shape of the tip.

In the [111] case there is only one appropriate glide cylinder available, therefore the prismatic loops repel, but do not react with each other, nor can they leave the tip. The [110] orientation, however, has two active glide cylinders with the same resolved shear stress. Thus reactions between prismatic loops on both cylinders are possible, leading to sessile dislocations, work hardening, and to the complex dislocation processes described in Sec. III A 2. Such dislocation reactions of course make the entire process irreversible.

The contact formed during retraction in the [110] oriented sample is nearly twice as long as the neck formed upon retraction of the [111] oriented tip. This is in part due to the larger contact area at beginning of the tip retraction (see Fig. 13), but mostly due to the fact that the dislocations can leave the tip, which is therefore easier deformed than the [111] tip. This can be seen in Fig. 6(b), which shows that the neck is almost fully formed out of atoms belonging initially to the tip.

The deformation mechanism of the neck changes when it reaches a certain size. For the [111]-oriented sample the deformation mechanism changed from nucleation of prismatic loops to homogeneous shear at a contact diameter of $\sim$2.5 nm. From $\sim$1.5 nm on the deformation is only carried by atomic rearrangements, see Fig. 5. Due to the partially hollow neck in the [110]-oriented configuration, the critical neck diameter cannot be determined easily, atomic rearrangements take place when the neck structures are 4–5 atoms wide. Similar changes in the deformation mechanism with decreasing contact diameter were reported for fcc metals.[21] There the crossover from slip by glide dislocations to homogeneous shear takes place at a contact diameter around 1.5 ± 0.3 nm. It was reasoned that this change in mechanism can be explained from the energy of the dislocations.[21] The energy of a prismatic dislocation of radius R and Burgers vector b scales as $R\ln(2R/b)$, whereas the energy required for homogeneous slip scales as R^2, which therefore can become more favorable as R is reduced.

The atomic rearrangements in thinner contacts take place mostly in the disordered part of the neck. This active zone can extend up to roughly five atomic planes. During elongation new ordered planes form from this active zone. In this process the atoms seem to accumulate in a way that extends the existing {110} planes, as can be seen during the final stage of the [111]-oriented neck, Fig. 5. The overall process of atomic rearrangements is similar to the one reported for fcc metals.[17,20,21]

The described plastic necking of the contact is contrary to the notion of tungsten being brittle at low temperatures. In fact, static calculations of crack propagation in a plate geometry using the same interatomic potential and stepwise loading show for cracks on (110) planes a critical stress intensity factor of only $K_{Ic}=1.6-2.2$ MPa $m^{1/2}$, depending on the crack front direction.[45] The potential therefore clearly allows fracture to take place. The perfectly matching, defect-free contact between tip and substrate can be seen as a notched, axisymmetric tungsten single crystalline tensile test sample. For quasistatic simulations brittle fracture of this setup could be expected. The contact, however, fails by plastic yielding. The nucleation and motion of prismatic dislocation loops allows the formation of a neck and its subsequent elongation. The dominance of this deformation mechanism is innate to the three-dimensional nature of the contact, its small scale and the adequate crystalline orientation. The formation of prismatic dislocation loops is favored by the radial symmetry of the stress concentration and by the small angle between glide cylinder axis and the direction of applied load. However, this mechanism is only expected for small contacts, as the energy of the prismatic dislocation loop is proportional to the contact radius a.

Prismatic dislocation loops as dominant deformation mechanism have some important implications for the plastic behavior. Most important is the lack of screw dislocations. In the low temperature regime the bulk plasticity of tungsten is believed to be controlled by the mobility of screw dislocations.[46] Because no screw dislocations are involved here, the prismatic dislocations are very mobile and provide an efficient way to accommodate the deformation and provide efficient shielding of the stress concentration between tip and substrate.

The high mobility of prismatic dislocation loops and the reduced possibility for dislocation reactions therefore lead to plastic rather than brittle response[47] of the contact under tensile loading. For macroscopic contacts, however, deformation must be carried by conventional glide dislocations, and their behavior should then compare to the brittle behavior of the bulk material.

Generation of prismatic dislocation loops could be a common feature of nanoscale stress concentrators with rotational symmetry (like notched cylinders or joints) in adequately oriented bcc metals. Nanoscale contacts might therefore show significantly more plastic deformation than expected from bulk deformation behavior, and this might lead to interesting implications for the mechanics of microscale contacts and for the adhesion in MEMS.

The simulations with matching tip-substrate orientations furthermore nourish the hope that the experimental study of tungsten nanocontacts might be possible, e.g., using adequately oriented single crystals in MCBJs. Previous MCBJ studies using a polycrystalline W wire broken at 4.2 K in an ultrahigh vacuum environment showed no adhesive neck formation.[6]

2. Configurations with different crystallographic orientations

The retraction of the tip from a substrate with different crystallographic orientation is significantly less complex. In all cases deformation takes place only within an active zone near the interface. Upon elongation, layers of atoms are formed out of the disordered zone. Eventually, the contact fractures at the interface without any prior dislocation activity.

Due to the curvature of the tip apex, the creation of (partial) layers is energetically favorable on the substrate. Therefore tip atoms in the active zone close to the substrate tend to adopt the crystallographic orientation of the substrate. In all the cases in which the tip was pushed against the substrate, debris with the crystallographic orientation of the substrate is left behind, see Fig. 12.

Transfer of mass has commonly been reported for simulations in which tip and substrate share the same crystallographic orientation.[11,14,16] However, the simulations show that the contact of asperities is an irreversible process, even in case of shallow indentation between crystallites of highly different crystallographic orientation. The formation of protrusions has to be taken into account when considering asperities that repeatedly contact a surface, as in the case of high-frequency MEMS switches.

For the configurations with different orientations of tip and substrate the load as well as the contact area as function of the displacement show reasonable agreement with the Hertzian expression. Furthermore, limited dislocation activity is only recorded in orientation IV, and all configurations show brittle fracture at the interface.

TABLE I. Properties of the used potential for tungsten (Refs. 34 and 35). Due to the isotropy of tungsten the same reduced modulus E^* can be used for the discussion of the different indenter-substrate configurations. $\gamma_{(110)}$ and $\gamma_{(111)}$ are the surface energies of (110) and (111) surfaces. $\gamma_{(111)}^{(110)}$ is the energy of a $(110)_I \| (111)_{II}; [1\bar{1}1]_I \| [1\bar{1}0]_{II}$ grain boundary, $\gamma_{(111)}^{(111)}$ the energy of a $(111)_I \| (111)_{II}; [0\bar{1}1]_I \| [1\bar{1}0]_{II}$ $\Sigma=3$ twist boundary.

Elastic constants (GPa)	c_{11}	522.4	c_{12}	204.4	c_{44}	160.6	E^*	222.3
Interface energies (mJ/m^2)	$\gamma_{(110)}$	2572	$\gamma_{(111)}$	3297	$\gamma_{(111)}^{(110)}$	3494	$\gamma_{(111)}^{(111)}$	2346

The brittle fracture of an adhesion joint was studied in the framework of the JKR theory[48] by Maugis and Barquins.[49] By calculating the strain energy release rate G and by applying Griffith's criterion $G=w$ (here w is the thermodynamic work of adhesion) they derived the critical load P_c and critical contact radius a_c at which under fixed loading conditions the contact will fracture

$$P_c = -\frac{3}{2}\pi w R, \tag{4}$$

$$a_c^3 = 3\pi w R^2 / 2E^*. \tag{5}$$

The work of adhesion can be expressed in terms of surface energies $\gamma_s^{1,2}$ of the contacting surfaces and the interfacial energy γ_{GB}^{12}:

$$w = \gamma_s^1 + \gamma_s^2 - \gamma_{GB}^{12}. \tag{6}$$

This approach, however, neglects the finite size of the interface curvature effects as well as possible changes in interface energy and structure.

The surface and interface energies are usually calculated for flat, ideal, and infinite interfaces (Table I). Whether these values can be used to determine w in Eq. (6) for atomic scale contacts is questionable, because the finite size and the curvature of the interface cannot be neglected at such small scales. A way to estimate the work of adhesion from the simulation data is to calculate the difference of potential energies between the starting configuration and the configuration when the tip touches the substrate and experiences no net forces: $w^{\text{est}} = (E_{\text{pot}}^{z=5} - E_{\text{pot}}^{P\approx 0})/A^{P\approx 0}$. This estimate takes into account the effects of the finite size of the interface, including the triple line at the surface, and of tip curvature. The so estimated work of adhesion and the work of adhesion

TABLE II. Work of adhesion w, maximal adhesive force predicted from continuum theory P_c^{est}, maximal adhesive force in the simulations P_c, and the change in interface energy W_{ind} during indentation and subsequent retraction for different combinations of crystallographic orientations of tip and substrate (see text).

Crystalline orientation	w^{calc} (eV Å^{-2})	w^{est} (eV Å^{-2})	P_c^{est} (nN)	P_c (nN)	W_{ind} (eV)
V	−0.27	−0.34	−128	−256	−140
V′	−0.27	−0.34	−128	−161	−140
III	−0.15	−0.41	−155	−239	−91
IV	−0.15	−0.36	−137	−219	−63

calculated from the ideal surface and interface energies [Eq. (6)] are shown in Table II. For some of the interfaces there are significant differences between both expressions for w. The different atomic structure of the tip apex leads to different values of w^{est} for the nominally equivalent interfaces $(111)_t \| (110)_s ; [1\bar{1}0]_t \| [1\bar{1}1]_s$ (orientation III) and $(110)_t \| (111)_s ; [1\bar{1}1]_t \| [1\bar{1}0]_s$ (orientation IV). The use of Eq. (6) to evaluate the work of adhesion thus is not adequate in the case of very small contact areas or radii of curvature.

The amount of irreversible changes of the interface during indentation and the following retraction can be quantified by evaluating the difference in potential energy between the two configurations at approximately zero load: $W_{\mathrm{ind}} = E_{\mathrm{pot}}^{P_{\mathrm{retr}} \approx 0} - E_{\mathrm{pot}}^{P_{\mathrm{ind}} \approx 0}$, see Table II. The configurations after indentation and subsequent retraction to $P \approx 0$ always have a lower potential energy compared to the configuration at $P \approx 0$ during indentation. It can be seen in Fig. 11 that this is mostly due to the increased contact area caused by the change of the tip shape. But W_{ind} will certainly also include changes in the interface energy due to structural rearrangements. The latter contribution is however difficult to evaluate since the actual interface area is somehow uncertain.

The use of w^{est} in Eq. (4) is adequate when the initial contact is submitted only to small changes. The fracture load P_c^{est} for configuration V' which was indented only to $z = -0.1$ nm calculated with Eq. (4) and $R = 5$ nm thus agrees reasonably well with the maximal adhesive force P_c during retraction. In all other cases using the initial radius of curvature $R = 5$ nm and w^{est} results in values of P_c^{est} that are significantly lower than the maximal adhesive force in the simulations, see Table II. This is expected to be a general aspect of nanoscale contact problems in which the atoms at the interface between the contacting bodies can significantly change the interface structure and energy by local rearrangements.

V. SUMMARY

In this paper the analysis of atomistic simulations of contact formation, indentation, subsequent pulling, and contact failure between a tungsten tip and a tungsten substrate is presented. The setup for the quasistatic simulations is chosen such that it mimics the indentation-retraction cycle of a displacement controlled STM tip at low temperatures. Different combinations of crystallographic orientations of tip and substrate are studied: [111] and [110] oriented tips indenting in a substrate with identical crystallographic orientation, as well as configurations which upon contact between indenter and substrate form large angle grain boundaries.

For the configurations with continuous crystallographic orientation relationship across the tip-substrate interface the deformation is dominated by the nucleation and glide of prismatic dislocation loops. The plastic behavior and the tendency to neck formation upon tip retraction is therefore primarily influenced by the availability and orientation of appropriate glide cylinders. The dominance of prismatic dislocation loops is innate to the three-dimensional nature of the contact and its small scale. Since no screw dislocations are involved in the deformation process, the plastic behavior differs significantly from the usual brittle behavior of bcc metals at low temperatures. The prismatic dislocation loops provide an efficient way of accommodating the deformation and thereby enable the formation of a connective neck instead of brittle fracture of the contact. Upon a certain neck diameter the deformation mechanism changes to neck elongation by atomic rearrangements within the neck, comparable to the processes during wire pulling in fcc metals.

In the case of configurations with different crystallographic orientations, the deformation during indentation and subsequent retraction is dominated by processes at the tip-substrate interface. In case these atomic rearrangements are small, they leave no signature in the load-displacement curve. Larger atomic rearrangements, however, lead to significant force drops. If these rearrangements are correlated, they can be accompanied by an elastic tilting of the tip. For the shallow indentations studied here, dislocation emission was observed in only one mismatching case.

Upon retraction the contact always fails at the interface. However, a significant amount of material is transferred from the tip to the substrate. The fact that even a shallow indentation and subsequent pulling of an asperity from a surface of the same metal is an irreversible process that has to be taken into account when considering repeated contact between two bodies.

The differences between the studied configurations in their tendency towards dislocation nucleation draws the attention towards the influence of the interface structure on nanotribological problems. The comparison of the maximal adhesive force sustained by the contacts between tip and substrate of different crystalline orientation with a continuum treatment of the fracture of an adhesive joint shows that due to the local rearrangements at the interface the concept of a *constant* interface energy cannot be applied to atomic scale metallic contacts under load, even when their overall behavior resembles to that of a Hertzian contact.

Although real world contact problems are much more complex than our model study, the present study underlines that atomistic aspects at the interface between contacting bodies become important at the nanoscale. In order to establish links to macroscopic observations and to provide interface-sensitive empirical functional formulations for a more realistic description of small scale contacts, a deeper understanding of the processes on the atomistic length- and time-scales involved in contact mechanics is desirable.

ACKNOWLEDGMENTS

The authors thank J. M. Wulveryck for suggesting the simulation geometry and M. Mrovec for performing the BOP calculation. They gratefully acknowledge partial financial support from the European Commission through the Marie-Curie Research Training Network "Complex Atom Modeling" (Contract No. HPRN-CT-2000-00154).

*Author to whom correspondence should be addressed. Electronic address: erik.bitzek@izbs.uni-karlsruhe.de

[1] F. P. Bowden and D. Tabor, *The Friction and Lubrication of Solids* (Clarendon Press, Oxford, 1950).
[2] B. Bhushan, J. N. Israelachvili, and U. Landman, Nature (London) **374**, 607 (1995).
[3] J. Gao, W. D. Luedtke, D. Gourdin, M. Ruths, J. N. Israelachvili, and U. Landman, J. Phys. Chem. B **108**, 3410 (2004).
[4] N. Agraït, A. L. Yeyati, and J. M. van Ruitenbeek, Phys. Rep. **377**, 81 (2003).
[5] C. J. Muller, J. M. van Ruitenbeek, and L. J. de Jongh, Phys. Rev. Lett. **69**, 140 (1992).
[6] A. Halbritter, S. Csonka, G. Mihály, E. Jurdik, O. Y. Kolesynchenko, O. I. Shklyarevskii, S. Speller, and H. van Kempen, Phys. Rev. B **68**, 035417 (2003).
[7] J. K. Gimzewski and R. Möller, Phys. Rev. B **36**, R1284 (1987).
[8] J. I. Pascual, J. Mendez, J. Gómez-Herrero, A. M. Baro, N. Garcia, U. Landman, W. D. Luedtke, E. N. Bogachek, and H. P. Cheng, Science **267**, 1793 (1995).
[9] N. Agraït, G. Rubio, and S. Vieira, Phys. Rev. Lett. **74**, 3995 (1995).
[10] G. Rubio-Bollinger, S. R. Bahn, N. Agraït, K. W. Jacobsen, and S. Vieira, Phys. Rev. Lett. **87**, 026101 (2001).
[11] M. Brandbyge, J. Schiøtz, M. R. Sørensen, P. Stoltze, K. W. Jacobsen, J. K. Nørskov, L. Olesen, E. Laegsgaard, I. Stensgaard, and F. Besenbacher, Phys. Rev. B **52**, 8499 (1995).
[12] U. Landman, W. D. Luedtke, N. A. Nurnham, and R. J. Colton, Science **248**, 454 (1990).
[13] T. N. Todorov and A. P. Sutton, Phys. Rev. Lett. **70**, 2138 (1993).
[14] A. Buldum, S. Ciraci, and I. P. Batra, Phys. Rev. B **57**, 2468 (1998).
[15] C. W. Yong, W. Smith, and K. Kendall, Nanotechnology **14**, 829 (2003).
[16] P.-R. Cha, D. Srolovitz, and T. K. Vanderlick, Acta Metall. Sin. **52**, 3983 (2004).
[17] A. M. Bratkovsky, A. P. Sutton, and T. N. Todorov, Phys. Rev. B **52**, 5036 (1995).
[18] U. Landman, W. D. Luedtke, B. E. Salisbury, and R. L. Whetten, Phys. Rev. Lett. **77**, 1362 (1996).
[19] R. N. Barnett and U. Landman, Nature (London) **387**, 788 (1997).
[20] H. Mehrez and S. Ciraci, Phys. Rev. B **56**, 12632 (1997).
[21] M. R. Sørensen, M. Brandbyge, and K. W. Jacobsen, Phys. Rev. B **57**, 3283 (1998).
[22] P. Jelínek, R. Pérez, J. Ortega, and F. Flores, Phys. Rev. B **68**, 085403 (2003).
[23] A. P. Sutton, Curr. Opin. Solid State Mater. Sci. **1**, 827 (1996).
[24] *Springer Handbook of Nanotechnology*, edited by B. Bhushan (Springer-Verlag, Heidelberg, 2004), Chap. C, p. 497.
[25] C. W. Yong, K. Kendall, and W. Smith, Philos. Trans. R. Soc. London, Ser. A **362**, 1915 (2004).
[26] S. S. Mani, J. G. Fleming, J. A. Walraven, J. J. Sniegowski, M. P. de Boer, L. W. Irwin, D. M. Tanner, D. A. LaVan, M. T. Dugger, J. Jakubczak, and W. M. Miller, *Proc. of the 38th Annual Inter. Reliability Phys. Symp. 2000* (IEEE, New York, 2000), pp. 146–151.
[27] D. K. Biegelsen, F. A. Ponce, J. C. Tramontana, and S. M. Koch, Appl. Phys. Lett. **50**, 696 (1987).
[28] I. Ekvall, E. Wahlström, D. Claesson, H. Olin, and E. Olsson, Meas. Sci. Technol. **10**, 11 (1999).
[29] E. Lilleodden, J. Zimmermann, S. Foiles, and W. Nix, J. Mech. Phys. Solids **51**, 901 (2003).
[30] K. J. Van Vliet, J. Li, T. Zhu, S. Yip, and S. Suresh, Phys. Rev. B **67**, 104105 (2003).
[31] J. A. Zimmerman, C. L. Kelchner, P. A. Klein, J. C. Hamilton, and S. M. Foiles, Phys. Rev. Lett. **87**, 165507 (2001).
[32] E. Bitzek, P. Koskinen, F. Gähler, M. Moseler, and P. Gumbsch (unpublished).
[33] http://www.itap.physik.uni-stuttgart.de/~imd (2002).
[34] M. W. Finnis and J. E. Sinclair, Philos. Mag. A **50**, 45 (1984).
[35] G. J. Ackland and R. Thetford, Philos. Mag. A **56**, 15 (1987).
[36] J. Li, Modell. Simul. Mater. Sci. Eng. **11**, 173 (2003).
[37] D. Rodney and G. Martin, Phys. Rev. B **61**, 8714 (2000).
[38] Y. Choi, K. J. Van Vliet, J. Li, and S. Suresh, J. Appl. Phys. **94**, 6050 (2003).
[39] M. Mrovec, V. Vitek, D. Nguyen-Manh, D. G. Pettifor, L. G. Wang, and M. Sob, in *Multiscale Phenomena in Materials—Experiments and Modeling*, edited by I. M. Robertson, D. H. Lassila, B. Devincre, and R. Phillips (Materials Research Society, Warrendale, PA, 2000), Vol. 578, p. 199.
[40] M. Mrovec (private communication).
[41] M. Vergeles, A. Maritan, J. Koplik, and J. R. Banavar, Phys. Rev. E **56**, 2626 (1997).
[42] B. Luan and M. O. Robbins, Nature (London) **435**, 929 (2005).
[43] D. E. Kramer, K. B. Yoder, and W. W. Gerberich, Philos. Mag. A **81**, 2033 (2001).
[44] C. R. Krenn, D. Roundy, M. L. Cohen, D. C. Chrzan, and J. W. Morris, Jr., Phys. Rev. B **65**, 134111 (2002).
[45] J. Riedle, P. Gumbsch, and H. F. Fischmeister, Phys. Rev. Lett. **76**, 3594 (1996).
[46] J. W. Christian, Metall. Trans. A **14A**, 1237 (1983).
[47] P. Gumbsch, J. Nucl. Mater. **323**, 304 (2003).
[48] K. L. Johnson, K. Kendall, and A. D. Roberts, Proc. R. Soc. London, Ser. A **324**, 301 (1971).
[49] D. Maugis and M. Barquins, J. Phys. D **11**, 1989 (1978).